Astronomical and Astrophysical Transactions (*AApTr*), 2016, Vol. 29, Issue 4, pp. 481–492,
ISSN 1055-6796, Photocopying permitted by license only, ©Cambridge Scientific Publishers

Radio emission of anomalous pulsars

I.F. Malov*

Pushchino Radio Astronomy Observatory, Astro Space Center, Lebedev Physical Institute, Russian Academy of Sciences, Pushchino, Moscow Region, 142290 Russia

Received 15 September, 2015

Our methods for calculations of angles between magnetic moments and rotation axes of neutron stars have been used for AXPs. The obtained values of these angles are small and give the possibility to use the drift model for the description of the known AXPs. The size of magnetospheres in nearly aligned rotators is much more than the radius of the light cylinder. In these conditions the cyclotron instability can develop and lead to the generation of transverse waves. The increment of this instability is large enough to provide the rather high power of radio emission. The spectrum of such emission is very steep (spectral index $\alpha > 3$). This is in good agreement with the known observations of AXPs ($\alpha > 2$). Moreover in these regions the synchrotron radiation can be generated with the maximum emission in the microwave range. The joint operating of the cyclotron instability and the synchrotron mechanism can explain the observed spectra of AXPs.

Keywords: Anomalous pulsars, drift model, radio emission

1 Introduction

Observations have revealed the existence of isolated neutron stars, registered as sources of pulsed radiation in various ranges of the electromagnetic spectrum. These have acquired the name anomalous pulsars, and include anomalous X-ray pulsars (AXPs), soft gamma-ray repeaters (SGRs), rotating radio transients (RRATs), X-ray dim isolated neutron stars (XDINSs), and central compact objects in supernova remnants (CCOs). Descriptions of the properties of these objects can be found, e.g., in [1]. Radio emission has been detected from at least a member of each of the above classes [2–6], so they can also be considered as various kinds of radio pulsars. The nature of the radio emission in different types of pulsars is a topic for a separate discussion. Here, we will consider only the possibility of describing the radio emission from AXPs and SGRs.

*Email: malov@prao.ru

The magnetar model has usually been used to describe their peculiarities. However there are some doubts in the necessity to suggest high values of magnetic field in these objects. Indeed some AXPs and SGRs with usual values of magnetic fields are known. These are

SGR 0418+5729	$B = 6.2 \times 10^{12}$ G	$P = 9.08$ sec,
SWIFT J1822.3-1606	$B \sim 2 \times 10^{13}$ G	$P = 8.44$ sec,
3XMM J185246.6+003317	$B < 4.1 \times 10^{13}$ G	$P = 11.56$ sec.

On the other hand there are nearly 20 radio pulsars with $B > 10^{13}$ G [7] without any signs of AXPs or SGRs. So, it is not enough to have a high magnetic field to be an AXP or SGR.

To explain some peculiarities in radiation of XDINSs it is necessary to suggest anisotropic distribution of temperature at their surfaces. This can be caused by the complex structure of magnetic fields in these regions. One of the possible reasons leading to small scales of magnetic structure is the Hall drift. As a result the existence of multipolar magnetic fields with higher inductions comparing with dipole ones is possible.

Archibald et al. [8] registered the sudden decreasing of angular velocity in AXP 1E 2259+586. It is difficult to explain such a phenomenon in the frame of the magnetar model predicting a permanent slowing down of the rotation. Unpinning of superfluid threads or star quakes lead to positive changes of the rotation frequency. This effect can be easily explained in the accretion model [9–10]. The antiglitch is explained by an sudden accretion from the debris disk around the neutron star or the propeller interaction with relic matter. It is quite enough to possess magnetic fields at the surface of order of 10^{12} G as in normal radio pulsars [11].

X-ray luminosities of AXP/SGR are up to three orders lower than luminosities of usual X-ray pulsars (similar to Her X-1) and can be provided by the accretion with three orders lower rates. Such accretion can be connected with fall-back-disks.

As for gamma bursts in SGRs they must be connected with non-equilibrium layers under the crust of the neutron star with a small mass [10]. Mixing up in these layers leads to the moving of some heavy nuclei to the crust. Here they become unstable, their destruction initiates a chain nuclear reaction and causes the nuclear explosion. The accumulation of accreting matter near magnetic poles of the neutron star can be a trigger for gamma bursts.

We put forward an alternative model [12]. At the periphery of the magnetosphere some transverse drift waves must exist. They modulate the direction of the propagation of radiation and an observer sees one pulse during the period of such drift waves (Fig. 1). The interval between successive pulses is equal to the period of these waves and must differ from the rotation period.

We have shown in [12] that the drift model can explain the X-ray emission with the observed interval between the successive pulses.

The basic suggestion of the drift model is equality of the maximum wave length of drift waves to the radius of the light cylinder $r_{LC} = \dfrac{cP}{2\pi}$. It has been suggested also that the pulsed X-ray radiation is generated by the synchrotron mechanism. These suggestions give the possibility to calculate the rotation period, its derivative and the magnetic field strength in the region of the emission generation.

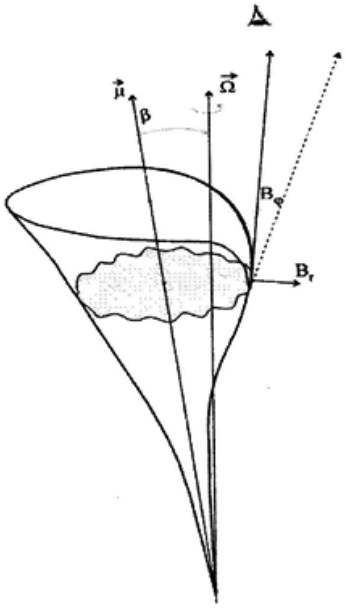


Figure 1 Scheme of the drift model. μ is the magnetic moment, Ω the rotation axis.

$$P(s) = 8.32 \times 10^{-2} \left[\frac{(\frac{dP_{dr}}{dt})_{-11}}{(L_x)_{34}(\frac{W}{P_{dr}})^2 P_{dr} f_{pl}} \right]^{\frac{2}{5}},$$

$$\frac{dP}{dt} = \frac{P\left(\frac{dP_{dr}}{dt}\right)}{2P_{dr}}, \tag{1}$$

$$B(G) = 22.45 \frac{P_{dr}}{P^2}.$$

Here P_{dr} and $\frac{dP_{dr}}{dt}$ are the observed interval between successive X-ray pulses and its measured derivative, L_x is the X-ray luminosity, $(L_x)_{34} = \frac{L_x(\text{erg/s})}{10^{34}}$, W is the measured pulse width (in seconds), $\left(\frac{dP_{dr}}{dt}\right)_{-11} = \frac{\frac{dP_{dr}}{dt}}{10^{-11}}$, f_{pl} the fraction of the pulsed X-ray emission.

The drift model can operate if the angle β between the magnetic moment and the rotation axis of the neutron star is small.

Here, we will not discuss some possible mechanisms for the generation of radio emission in the framework of the magnetar model, proposed, e.g., in [13–15] (a brief analysis of such mechanisms is given in [16]), and we consider only how the observed radio properties of AXPs can be explained by the drift model.

2 Main peculiarities of radio emission from AXPs and SGRs

Five AXPs have been detected in the radio: 1E 2259+586 [17], XTE J1810-197 [18], 1E 1547-5408 [19], 4U 0142+61 [20], and PSR J1622-4950 [21]. The 111-MHz flux density of 1E 2259+586 is $S_{111} = 35 \pm 25$ mJy, and upper limits have been obtained at 87 MHz, $S_{87} < 150$ mJy [17], 600 MHz, $S_{600} < 2.3$ mJy [22], and 1500 MHz, $S_{1500} < 0.05$ mJy [23]. These data show the very steep radio spectrum for this object, with a spectral index $\alpha > 2.5$. The radio luminosity of 1E 2259+586 is $L < 3 \times 10^{28}$ erg/s [23].

Strong variations are observed in the 111-MHz flux of 1E 2259+586, together with a very narrow pulse profile: the half-maximum level corresponds to only 1.7% of the pulse separation (6.98 s). In addition, a powerful interpulse is observed in the X-ray, and the main pulse occupies $\sim 27\%$ of the period [24] (whereas it is absent at meter wavelengths). A very narrow pulse (2.6% of the period) is also observed in the AXP 4U 0142+61 at 111 MHz; the X-ray pulse occupies $\sim 35\%$ of the period. As in 1E 2259+586, strong flux-density variations are observed at meter wavelengths. The measured mean flux density at 111 MHz is $S_{111} = 30 \pm 20$ mJy, and the upper estimates at higher frequencies ($S_{1400} < 0.3$ mJy [25] and $S_{1380} < 0.046$ mJy [26]) lead to a lower limit of the spectral index ($\alpha > 2.7$) and an upper limit of the radio luminosity ($L < 1.5 \times 10^{27}$ erg/s).

The AXP XTE J1810-197 has been observed over a broad range of radio frequencies, from 690 MHz to 144 GHz [27-32]. Strong fluctuations of the flux density, pulse shape, pulse arrival times, and spectral index have been detected. The high linear polarization of the emission (from 85 to 90%) has made it possible to obtain the swing of polarization position angle within the pulse. The maximum derivative of the polarization position angle ψ with respect to the longitude Φ is about unity [31]. In the standard model, in which the ψ variations are due to the line of sight crossing different projections of magnetic field lines, the maximum derivative should be

$$C = \left|\frac{d\psi}{d\Phi}\right|_{max} = \frac{\sin\beta}{\sin(\zeta - \beta)}, \tag{2}$$

where ζ is the angle between the line of sight and the spin axis. The quantity $\zeta - \beta$ is the minimum angular distance between the line of sight and the center of the radiation cone, and cannot be larger than the radius of this cone. The formula (2) has been obtained in the frame of the Rotating Vector Model. In the drift model the line of sight crosses successive field lines as well. The exact expression similar to (2) is not obtained yet in this model. However both angles (ζ and β) must be small in its frame also. In the standard model, the cone size is of the order of 10°–20°. Therefore, if $C \sim 1$, the angle β should be not larger than 10°–20°, and the pulsar is a nearly aligned rotator. The detection of an interpulse in this pulsar, separated by approximately 240° but not 180° [33] may also testify to a close to aligned geometry.

The average flux density at 62 MHz is $S = 160\,mJy$ [34]. Taking into account the measurements at the higher frequency[31], this yields the spectral index $\alpha = 2.2$. As in the case of the AXP XTE J1810-197, the polarization data for 1E 1547-5408 indicate a small derivative C [35], again testifying to a small angle β. In [31] and [35] the authors conclude that their results do not contradict the aligned geometry of XTE J1810-197 and 1E 1547-5408. Thus, summarizing the above observational results, the

radio spectra for known AXPs are steep, and there is evidence that the inclination of the magnetic moment (identified in standard pulsar models with the axis of the radiation cone) to the spin axis of the neutron star is small. The fact that very broad X-ray pulses are observed in all AXPs also suggests that these objects are nearly aligned rotators. Narrow radio pulses are observed. They correspond to expectations of the drift model and give the possibility to use it for the further analysis.

3 The model

We will use PSR J1622-4950 as a standard AXP. In this pulsar, the interval between the observed successive pulses is $P = 4.3$ s, and the surface magnetic field calculated using the magnetic-dipole formula is $B_s \sim 4 \times 10^{14}$ G. Strong flux variability and pulse shape variations are characteristics of this object, as well as large variations in the pulse arrival time. These properties are observed in all AXPs, and PSR J1622-4950 is very similar to XTE J1810-197 and 1E 1547-5408. According to polarization measurements, the angle β in PSR J1622-4950 is 15.6° [36], i.e., it is also an aligned rotator, and the drift model is applicable. This model yields the estimated rotation period $P = 0.32$ s, period derivative $dP/dt = 6.29 \times 10^{-13}$, magnetic field in the region of generation of the radiation $B = 950$ G, and surface magnetic field for the dipole structure in all magnetosphere $B_s = 3.4 \times 10^{12}$ G [36]. This value has been obtained using $B = 950$ G near the light cylinder and the suggestion on the dipole structure of the magnetic field from the surface up to the periphery of the pulsar magnetosphere. This B_s differs from the magnetodipole value $B_s = 6.4 \times 10^{19}\sqrt{P\frac{dP}{dt}} = 2.8 \times 10^{13}$ G. It means that there are some other braking mechanisms (for example, pulsar winds [37]). The magnetosphere – the region where the plasma processes that are most important for the formation of the observed radiation occur – extends much farther in pulsars with small angles β than in pulsars with large inclinations of their magnetic moments relative to their spin axes. Indeed, the distance at which the radiation cone axis reaches the light cylinder is (Fig. 2)

$$r_* = \frac{r_{LC}}{\sin\beta}. \tag{3}$$

For $\beta = 15.6°$, the boundary of the magnetosphere corresponds to $r_* \approx 4r_{LC}$. The large extent of the magnetosphere makes it possible to avoid difficulties that arise in the application of mechanisms for the cyclotron instability and the formation of appreciable pitch angles for the radiating electrons in models in which the magnetosphere is restricted to the light cylinder radius (see, e.g., [38]). It was shown in [39] that the dispersion equation describing the behaviour of transverse waves in the upper layers of the pulsar magnetosphere is

$$\frac{1}{2\gamma_r^2} + \frac{1}{2}\left(\frac{k_x}{k_\varphi} - \frac{u_x}{c}\right)^2 + \frac{k_r^2}{2k_\varphi^2} - \delta = \pm\frac{\omega_B}{\gamma_r k_\varphi c}. \tag{4}$$

Here, γ_r is the Lorentz factor of the resonance particles, $\omega_B = eB/mc$ is the cyclotron frequency, k_i are the components of the wave vector in the cylindrical coordinates, u_x is the drift velocity of particles, and

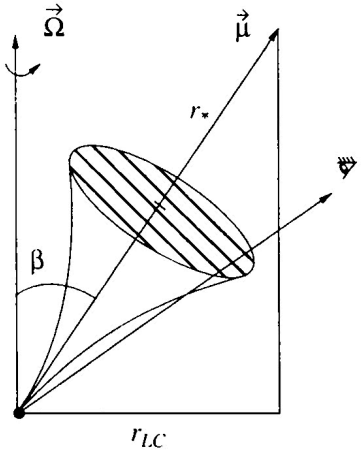


Figure 2 The model of the magnetosphere.

$$\delta = \frac{\omega_p^2}{4\gamma_p^3 \omega_B^2}, \tag{5}$$

where $\omega_p^2 = 8\pi n_p e^2/m$ is the square of the plasma frequency. A plus sign on the right-hand side of (4) corresponds to attenuation via the normal Doppler effect, and a minus sign to emission via the anomalous Doppler effect. As follows from (4), this emission requires that

$$\delta > \frac{1}{2\gamma_r^2} + \frac{1}{2}\left(\frac{k_x}{k_\varphi} - \frac{u_x}{c}\right)^2 + \frac{k_r^2}{2k_\varphi^2}, \tag{6}$$

which corresponds to the generation of waves at the frequency

$$\omega = \frac{4\gamma p^3 \omega B^3}{\gamma_r \omega_p^2}, \tag{7}$$

where γ_p is the Lorentz factor of the particles of the secondary plasma (Fig. 3).

Under the assumptions that are standard for the adopted magnetosphere models, the ratio of the distance where radiation with the frequency (7) is generated to the radius of the neutron star is [36]

$$\frac{r}{R_*} = \left(\frac{e^2 B_s^2 P \gamma_p^4}{2\pi^2 m^2 c^2 \gamma_b^2 \nu}\right)^{1/6} = 1.42 \cdot 10^3 \left(\frac{P B_{12}^2}{\nu_8}\right)^{1/6}. \tag{8}$$

Here, γ_b is the Lorentz factor of the primary-beam electrons.

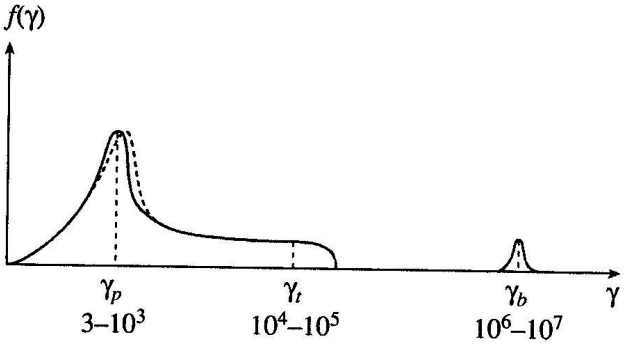


Figure 3 Distribution functions of the electrons(solid)and positrons(dashed) in the pulsar magnetosphere [40].

4 Results

With the values of P and B derived for PSR J1622-4950, we obtain

$$\frac{r}{R_*} = \frac{1.76 \times 10^3}{\nu_8^{1/6}}. \tag{9}$$

The increment of the cyclotron instability was calculated in [39]:

$$\Gamma = \frac{\pi \omega_{pres}^2}{\omega \gamma_T}, \tag{10}$$

where ω_{pres} is the plasma frequency of the resonance particles and γ_T is the thermal scatter of their Lorentz factors. We showed in [36] that a sufficient amplification of waves is possible in the outer layers of the magnetosphere only if the resonance particles are electrons in the tail of the distribution for the secondary plasma, with Lorentz factors $\gamma_t \sim 10^4$–10^5. Substituting the corresponding expressions into (10) yields

$$\Gamma_{ct} = \frac{2\pi e B_s \gamma_b (R_*/r)^3}{mcP\nu\gamma_T\gamma_t}. \tag{11}$$

Setting $\gamma_b = 10^7$, $\gamma_t = 10^5$, and $\gamma_T = 100$, we find the increment

$$\Gamma_{ct} = 1.17 \times 10^{13} (R_*/r)^3 \nu_8^{-1}. \tag{12}$$

We can estimate the efficiency of the wave amplification using the quantity

$$\tau_{ct} = \int \Gamma_{ct} \frac{dr}{c}, \tag{13}$$

which, with the chosen parameter values, is

$$\tau_{ct} = 1.17 \times 10^{13} \nu_8^{-1} \int \frac{dx}{x^3}, \tag{14}$$

where

$$x = \frac{r}{R_*}. \tag{15}$$

Taking $R_* = 10^6$ cm, which yields $r_{LC} = 1.53 \times 10^9$ cm, and assuming the generation region to be confined between $x_1 = 1.76 \times 10^3$ and $x_2 = 3r_{LC} = 4.59 \times 10^3$, we obtain

$$\tau_{ct} = 13.5\nu_8^{-1}. \tag{16}$$

Relationship (9) means that the radiation at lower frequencies is generated higher in the magnetosphere. If the number density of the radiating electrons continues to decrease as $n \propto r^{-3}$, as in a dipole field, and the intensity increases proportional to the wave amplitude, then, taking into account (9) and (16), we obtain a ratio for the intensities at 100 MHz and 1 GHz of the order of 10^4, which corresponds to a spectral index $\alpha = 3.8$. The spectra of the three AXPs considered above are indeed very steep ($\alpha > 2.2$), consequently, these sources were successfully detected at 100 MHz, but not at frequencies of the order of 1 GHz.

5 The role of synchrotron radiation

We obtained the solution of the kinetic equation for the distribution function of relativistic electrons taking into account their interactions with waves and radiation processes in [41]. This solution can be used to estimate the pitch angle of the radiating particles, which, in the adopted notation, is

$$\Psi_0 = \left(\frac{3\pi^3 m^5 c^7 \gamma_b^3}{4e^6 B_s^4 P^3 \gamma_p^4 \gamma_r^2}\right)^{1/4} \left(\frac{r}{R_*}\right)^3. \tag{17}$$

Substituting the numerical values of the parameters and fundamental constants, we obtain

$$\Psi_0 = 3.73 \times 10^{-12} (r/R_*)^3. \tag{18}$$

Here we have adopted $\gamma_p = 8.5$ for the Lorentz factor of the secondary plasma, $\gamma_r = 5 \times 10^4$ for the average Lorentz factor of the resonance particles in the tail of the distribution, and $\gamma_b = 10^7$ for the primary beam. With the above distances for the generation of radiation, $x_1 = 1.76 \times 10^3$ and $x_2 = 4.59 \times 10^3$, we obtain from (18) $\Psi_0 = 0.025 - 0.446$ rad. Using the formula for the frequency of the maximum of the synchrotron spectrum of a single electron (see, e.g., [42], p. 237)

$$\nu_{max} = \frac{0.87\omega\gamma^2 \sin\Psi_0}{4\pi}, \tag{19}$$

where γ is the Lorentz factor of the radiating particles, we find for PSR J1622-4950

$$\nu_{max} = 4.14 \times 10^{18} (R_*/r)^3 \gamma^2 \sin\Psi_0. \tag{20}$$

With the calculated distances and pitch angles, we obtain

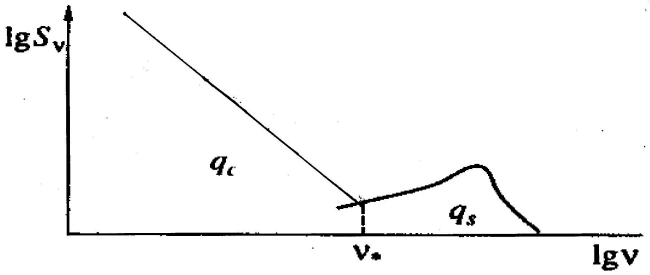


Figure 4 Schematic representation of the expected AXP spectrum, where q_c is the power of the waves generated due to the cyclotron instability and q_s is the synchrotron power.

$$\nu_{max} = (1.52 - 1.85) \times 10^7 \gamma^2 \,\mathrm{Hz}. \tag{21}$$

Figure 3 shows that there are segments in the electron distribution with different values of γ. However, the largest number of particles corresponds to the secondary plasma. For $\gamma = 100$, for example, the synchrotron spectrum peak is at $\nu_{max} \sim$ 150–200 GHz. With a monoenergetic distribution of radiating electrons, the intensity decreases toward lower frequencies as $\nu^{1/3}$ [42, p. 237], and the observed flux is expected to grow with frequency at frequencies of tens of GHz (Fig. 4). Indeed, a flux increasing toward higher frequencies is observed near 10 GHz in XTE J1810-197 [30], and a similar increasing above 20 GHz is noted in 1E 1547-5408 [35].

6 Conclusions

The main conclusions of this study are the following.

1. Estimation of the angle β between the spin axis and magnetic moment of a neutron star together with observational data for AXPs has shown that these objects are close to aligned rotators, and that the drift model can be applied to them.

2. The magnetospheres of aligned rotators are appreciably more extended than in pulsars with large values of β. The ratio of the corresponding sizes is $\sin\beta_1 / \sin\beta_2$.

3. The conditions for the generation of transverse waves due to the cyclotron instability become more favorable in magnetospheres with such extents. The expected radiation spectrum is very steep (with spectral indices $\alpha > 3$). This mechanism can explain the observed radio spectra of the known AXPs (with $\alpha > 2$).

4. A large magnetosphere also favors the appearance of appreciable pitch angles for relativistic electrons, and hence the emission of synchrotron radiation. The maximum of this emission is in the microwave range. This mechanism can provide the observed fluxes at tens of GHz, and can explain the observed enhancement in the AXP emission in this range.

We also note the following. The relationships (20)–(21) demonstrate that the factors $(R_*/r)^3$ and $\sin\Psi_0$ essentially cancel each other, so that, for a given γ, the synchrotron peak is at the same frequency in the entire region where this emission is generated. However, we emphasize that the density of the radiating particles decreases with distance according to a cubic law, and maintaining appreciable radiated power

would require that more energetic electrons be involved (the factor of γ^2 in the above relationships). Such electrons do exist in the magnetosphere (Fig. 3), so that it may be quite possible to maintain the observed flux density.

We have used data for PSR J1622-4950 and compared the expected spectrum with the observed spectra of XTE J1810-197 and 1E 1547-5408 (PSR J1550-5418). The spectra of particular AXPs should be calculated using their individual data. A comparison of these spectra with other parameters of these objects and an analysis of their common features and differences is a subject of our future research.

Acknowledgements

This work was supported by the Basic Research Program of the Presidium of the Russian Academy of Sciences "Transitional and Explosive Processes in Astrophysics" (P-41) and the Russian Foundation for Basic Research (grant 16-02-00954). The author thanks L.B. Potapova for help with the preparation of the manuscript.

References

[1] I.F. Malov and G.Z. Machabeli (2009) Anomalous Pulsars Moscow: Nauka (in Russian)
[2] Yu.P. Shitov, V.D. Pugachev, S M. Kutuzov (2000) ASP Conf. Ser. 202, 685
[3] V.M. Malofeev, O.I. Malov, D.A. Teplykh, A.P. Glushak (2005) Astron. Telegram, 501, 1
[4] M.A. McLaughlin, J.R. Stairs, A.G. Lyne et al. (2006) Nature 591, L135
[5] F. Camilo, S.M. Ransom, J.P. Halpern et al. (2006) Nature 442, 892
[6] V.M. Malofeev, O.I. Malov, D.A. Teplykh (2007) Ap&SS 308, 211
[7] R.N. Manchester, G.B. Hobbs, A. Teoh, M. Hobbs (2005) AJ 129, 1993
[8] R. F. Archibald, V.M. Raspi, C.-Y. Ng et al. (2013) Nature 497, 591
[9] J.E. Truemper, K. Dennerl, N.D. Kylafis et al. (2013) ApJ 764, 49
[10] G.S. Bisnovatyi-Kogan, N.R. Ikhsanov (2014) ARep. 58, 217
[11] J.I. Katz Astro-ph.HE: 1307.0586v2
[12] I.F. Malov, G.Z. Machabeli (2006) A&AT 25, 7
[13] M. Lyutikov (2002) ApJL 580, L65
[14] C. Thompson (2008) ApJ 688, 499
[15] C. Thompson (2008) ApJ 688, 1258
[16] I.F. Malov (2010) ARep 54, 925
[17] V.M. Malofeev, O.I. Malov, D.A. Teplykh et al. (2005) ARep 49, 242
[18] J.P. Halpern, E.V. Gotthelf, R.H. Becker et al. (2005) ApJL 632, L29
[19] F. Camilo, S.M. Ransom, J.P. Halpern et al. (2007) ApJ 666, l93
[20] V.M. Malofeev, D.A. Teplykh, O.I. Malov (2010) ARep 54, 995
[21] L. Levin, M. Bales, S. Bates et al. (2010) ApJL 721, L33
[22] D.R. Lorimer, A.G. Lyne, F. Camilo (1998) A&A 331, 1002
[23] M.J. Coe, Z.R. Jones, H. Lehto (1994) MNRAS 270, 179
[24] S.K. Patel, C. Kouveliotou, P.M. Woods et al. (2001) ApJL 563, L45
[25] B.M. Gaensler, P.O. Slane, E.V. Gotthelf et al. (2001) ApJ 559, 963
[26] P.R. den Hartog, B. Kuiper, W. Hermsen et al. (2007) Ap&SS 308, 647

[27] F. Camilo, S.M. Ransom, J.P. Halpern et al. (2006) Nature 442, 892
[28] F. Camilo, J. Reynolds, S. Johnston et al. (2007) ApJL 659, L37
[29] F. Camilo, I. Cognard, S.M. Ransom et al. (2007) ApJ 663, 497
[30] F. Camilo, S.M. Ransom., J. Penalver et al. (2007) ApJ 669, 561
[31] M. Kramer, B.W. Stappers, A. Jessner et al. (2007) MNRAS 377, 107
[32] K. Lazaridis, A. Jessner, M. Kramer et al. (2008) MNRAS 390, 839
[33] M. Serylak, B.W. Stapers, P. Weltevrede et al. (2009) MNRAS 394, 295
[34] V.M. Malofeev, D.A. Teplykh, S.V. Logvinenko (2012) ARep 56, 35
[35] F. Camilo, J. Reynolds, S. Johnston et al. (2008) ApJ 679, 681
[36] I.F. Malov (2012) ARep 56, 29
[37] A.K. Harding, I. Contopoulos, D. Kazanas (1999) ApJ 525, 125
[38] G.Z. Machabeli, V.V. Usov (1989) SvAL 15, 393
[39] A.Z. Kazbegi, G.Z. Machabeli, G.I. Melikidze, in Magnetospheric Structure and Emission Mechanisms of Radio Pulsars, Ed. T.H. Hankins, J.M. Rankin, and J. A.Gil (Pedagogical Univ. Press, 1992), p. 232
[40] J. Arons, in Plasma Astrophysics, Ed. by T. D. Guyenne and G. Levy, ESA SP-161 (European Space Agency, Paris, 1981), p. 273
[41] I.F. Malov, G.Z. Machabeli (2002) ARep 46, 684
[42] G. Bekefi (1966) Radiation Processes in Plasma, New York: Wiley and Sons